Synthesis, structure and electrochemical properties of $LiNaCo_{0.5}Fe_{0.5}PO_4F$ fluoride-phosphate

Reference:

Fedotov Stanislav S., Kuzovchikov Sergey M., Khasanova Nellie R., Drozhzhin Oleg A., Filimonov Dmitriy S., Karakulina Olesia, Hadermann Joke, Abakumov Artem M., Antipov Evgeny V..- Synthesis, structure and electrochemical properties of $LiNaCo_{0.5}Fe_{0.5}PO_4F$ fluoride-phosphate

Journal of solid state chemistry - ISSN 0022-4596 - (2016), p. 1-8

Full text (Publishers DOI): http://dx.doi.org/doi:10.1016/j.jssc.2016.02.042

Synthesis, structure and electrochemical properties of $LiNaCo_{0.5}Fe_{0.5}PO_4F$ fluoride-phosphate

Stanislav S. Fedotov[a,b,*], Sergey M. Kuzovchikov[a], Nellie R. Khasanova[a], Oleg A. Drozhzhin[a], Dmitriy S. Filimonov[a], Olesia M. Karakulina[c], Joke Hadermann[c], Artem M. Abakumov[a,b,c], Evgeny V. Antipov[a]

[a] Department of Chemistry, Lomonosov Moscow State University, 119991 Moscow, Russian Federation

[b] Skoltech Center for Electrochemical Energy Storage, Skolkovo Institute of Science and Technology, 143026 Moscow, Russian Federation

[c] EMAT, University of Antwerp, Groenenborgerlaan 171, B-2020, Antwerp, Belgium

Abstract

$LiNaCo_{0.5}Fe_{0.5}PO_4F$ fluoride-phosphate was synthesized via conventional solid-state and novel freeze-drying routes. The crystal structure was refined based on neutron powder diffraction (NPD) data and validated by electron diffraction (ED) and high-resolution transmission electron microscopy (HRTEM). The alkali ions are ordered in $LiNaCo_{0.5}Fe_{0.5}PO_4F$ and the transition metals jointly occupy the same crystallographic sites. The oxidation state and oxygen coordination environment of the Fe atoms were verified by ^{57}Fe Mössbauer spectroscopy. Electrochemical tests of the $LiNaCo_{0.5}Fe_{0.5}PO_4F$ cathode material demonstrated a reversible activity of the Fe^{3+}/Fe^{2+} redox couple at the electrode potential near 3.4 V and minor activity of the Co^{3+}/Co^{2+} redox couple over 5 V vs Li/Li^+. The material exhibits a good capacity retention in the 2.4÷4.6 V vs Li/Li^+ potential range with the delivered discharge capacity of more than 82% (theo.) regarding Fe^{3+}/Fe^{2+}.

Highlights

- Freeze-drying method was successfully applied to the synthesis of $LiNaCo_{0.5}Fe_{0.5}PO_4F$ fluoride-phosphate.
- The crystal structure of $LiNaCo_{0.5}Fe_{0.5}PO_4F$ was refined based on NPD and validated by ED and HRTEM.
- The $LiNaCo_{0.5}Fe_{0.5}PO_4F$ cathode material demonstrated a reversible Li de/intercalation in the 2.5÷4.6 V vs Li/Li^+ potential range.

Keywords Li-ion batteries, fluorophosphates, high-voltage cathode, neutron diffraction

Introduction

Li-ion batteries provide a number of advantages over the existing energy storage technologies in terms of size, energy density, cycle life and power. Nowadays this technology not only takes part in shaping wireless devices but also conquers grid application niches. A crucial part that dominates the functional properties of Li-ion batteries as well as the price is the cathode [1,2]. In chase of low-cost, environmentally benign and chemically stable cathode materials, a huge variety of candidates was thoroughly scrutinized starting from simple layered oxides to complex polyanion and mixed anion compounds. At the same time, the crystal structure of the cathodes has evolved from close packings into much more sophisticated arrangements, which opened up ample opportunities to tune their electrochemical properties. The substitution within the metal cation sublattice drastically influences the delivered capacities and operating voltages and even alters the mechanism of the alkali ion extraction/insertion [3-6]. In many cases minor metal doping enables stabilizing different crystal structures with unique electrochemical performance [7,8]. The combination of different transition metals with particular electrochemical activities appeared to be a viable strategy in the search for new cathode materials. The other way towards the enhancement of cathode characteristics lies in the substitution within the anion sublattice or, in other words, combining two or more anion moieties [9,10]. In this case, fluoride-containing mixed-anion materials have drawn specific attention owing to the increase of the working potential compared to their oxide counterparts, anticipated better kinetics due to a lower affinity of lithium to fluorine than oxygen and richer structural diversity. A phosphate group chosen as a second anionic species is able to provide structural, thermal and chemical stability of the materials. Hence, fluoride-phosphate materials with $AMPO_4F$ (A = Li, Na; M = V, Fe) and A_2MPO_4F general formulae (A = Li, Na; M = Mn, Fe, Co, Ni) have been rigorously examined recently [11-22].

The interest in the A_2MPO_4F class was also ignited by the theoretical possibility of utilizing a multi-electron redox process with a reversible de/intercalation of more than one alkali ion doubling the specific capacity. In this series, the most attractive cathode containing earth-abundant elements, namely Li_2FePO_4F, crystallizes in three different polymorphs, which cannot be obtained directly due to their metastable crystal structures. Thus, the Li_2FePO_4F polymorph with a 3D framework [17] can be prepared through electrochemical ion exchange from isostructural conventionally synthesized $LiNaFePO_4F$. This, so-called "stacked" Li_2FePO_4F, exhibits a reversible electrochemical activity at an average potential of 3.4 V vs Li/Li^+ in contrast to the high-voltage electrochemical behavior of the cobalt-containing counterpart Li_2CoPO_4F [18,19], which demonstrates a reversible de/intercalation of lithium above 4.8 V vs Li/Li^+ (beyond the stability window of commercial electrolytes).

The substitution effect of Fe by Co in the stacked Li_2FePO_4F was estimated *ab initio* [20], it revealed that a partial replacement of Co by Fe in $Li_2Fe_{1-x}Co_xPO_4F$ might lower the average potential of the material in comparison to the pure Li_2CoPO_4F thereby adjusting it to the values sustained by conventional electrolytes. Furthermore, density states analysis for $Li_2Fe_{0.5}Co_{0.5}PO_4F$ brought out a strong hybridization for Fe-3d, Co-3d bands near the Fermi level, which implies that the Co-doped $Li_2Fe_{1-x}Co_{1-x}PO_4F$ may possess better electronic conductivity than the pure phase. These two points are worth

validating, since these features may result in enhanced electrochemical properties of the resulting cathode material such as better energy density and power parameters.

Our previous investigation of $Li_2Fe_{1-x}Co_xPO_4F$ fluoride-phosphates disclosed the presence of a limited solid solution ($0.7 \leq x \leq 1$) [21]. A further raise of the Fe content ($x < 0.7$) is thermodynamically unfavorable, however it is still possible once the simultaneous replacement of Li by Na takes place. Introduced to the structure, sodium ions play an important role in maintaining the fluoride-phosphate framework by pillaring the continuous tunnels [17]. To investigate the effect of the substitution on the electrochemical properties of these fluoride-phosphates we chose the $LiNaFe_{0.5}Co_{0.5}PO_4F$ composition with half-mixing in the transition metal sublattice. To obtain $LiNaFe_{0.5}Co_{0.5}PO_4F$ and the corresponding electrode material we used different synthesis: conventional solid-state and freeze-drying routes. Here, the latter technique was applied to the synthesis of fluoride-phosphate materials for the first time. It allowed combining two essential approaches to enhance the conductivity and, therefore, electrode performance: carbon coatings and nanostructuring, which led to materials with superior capabilities compared to conventional ceramic methods [23-25]. In this paper, we use this approach for the synthesis of $LiNaCo_{0.5}Fe_{0.5}PO_4F$ fluoride-phosphate with mixed occupancies in the metal sublattice and report on its crystal structure and electrochemical properties.

Experimental

Sample preparation

All of the reagents used in the syntheses were tested by means of X-ray powder diffraction (XPD), the hydrate water content was determined by thermal gravimetric analysis.

The $LiNaCo_{0.5}Fe_{0.5}PO_4F$ sample was synthesized via a two-step conventional solid-state method. First, $LiCo_{0.5}Fe_{0.5}PO_4$ was prepared as described in Ref. [26]. Then stoichiometric amounts of $LiCo_{0.5}Fe_{0.5}PO_4$ and NaF (99.9%) were mixed in a ball-milling machine (Fritch Pulverisette) in acetone media for 3 hours (200 rpm), pelletized and annealed under an argon flow at 625°C for 1 h followed by quenching to room temperature. For the freeze-drying method, the initial reagents (Li_2CO_3 (99%), $Co(NO_3)_2{\cdot}5.6H_2O$ (99%), $NH_4H_2PO_4$ (99.5%)) were dissolved in distilled water to form a transparent solution. The fine iron powder was dissolved in a 10% excess of HNO_3 (15% mass solution) at 80°C. The resulting light-brown solution was cooled down to room temperature and ascorbic acid was added serving as both an organic additive and reducer. 1M CH_3COOH was used to control the pH in the 3÷3.5 range. The third solution was prepared from equimolar NaF and NH_4F (99%) so that the molar ratio of Na:Co:F was 1:1:2. The three solutions were combined together and pulverized into liquid nitrogen, then placed into a vacuum sublimation machine Labconco Freezone 7948030. The pressure was kept at 0.1–0.3 mbar and the temperature was gradually increased from −40 to +30°C during 48 hrs. The final granulated powder was pressed into pellets and annealed at 350°C for 5 hours in a flow of high purity Ar to decompose the organics and remove volatile components. The product was ball-milled and annealed at 600°C in an argon flow for 1 hour with immediate quenching to room temperature.

Materials characterization

High-resolution synchrotron X-ray powder diffraction (SXPD) data were collected at the ID31 beamline of the European Synchrotron Radiation Facility (ESRF, Grenoble, France) using a wavelength of 0.40006 Å and eight scintillation detectors, each preceded by a Si (111) analyzer crystal. The powder sample was contained in a thin-walled quartz capillary, which was spun during the experiment.

Room temperature neutron powder diffraction (NPD) data were collected with the high-resolution powder diffractometer HRPT [Paul Scherrer Institute (PSI), Switzerland] at the wavelength of 1.494 Å. The Rietveld refinement of the $LiNaCo_{0.5}Fe_{0.5}PO_4F$ structure from NPD data was performed in JANA2006 program [27].

Electron diffraction (ED) and high-resolution transmission electron microscopy (HRTEM) study was carried out using a FEI Tecnai G2 electron microscope operated at 200 kV. Electron dispersive X-ray analysis (EDX) was conducted at a Philips CM 20 electron microscope (200 kV) using an Oxford Instruments detector. The specimen for the TEM study was prepared by grinding the sample under ethanol and depositing a few drops of the suspension onto a copper grid covered with a holey carbon layer. The experimental HRTEM image was filtered using a low bandpass filter and the theoretical one was calculated using a defocus and thickness of resp. 31 nm and 6.3 nm.

The morphology and particle size of the material were investigated by scanning electron microscopy (SEM) on a Supra 50 VP LEO (LaB_6-cathode, In-Lens-detector, 10÷20 kV) electron microscope. All the samples were preliminary coated with a 10 nm layer of metallic chromium by magnetron sputtering in Ar-plasma (Quorum Technologies Q150T Turbo-Pumped Sputter Coater / Carbon Coater).

Thermal analysis of the prepared samples was carried out with a (TG-DSC) STA-449 apparatus (Netzsch, Germany) under argon/oxygen flow (80:20 vol.). The powders were heated at 5÷10 K/min rate in the 25÷600°C temperature range.

^{57}Fe Mössbauer spectra of $LiNaCo_{0.5}Fe_{0.5}PO_4F$ were collected at room temperature with a ^{57}Co/Rh γ-ray source in a transmission mode. The velocities were calibrated with a high purity standard α-Fe absorber. Isomer shifts were related to α-Fe. The experimental data were fitted using the software "UnivemMS" [28].

Electrochemical measurements

The positive electrodes were prepared by thorough mixing of 75% active material, 10% carbon black (Carbon Super-C) and 15% polyvinylidene fluoride (PVdF) in N-methyl-pyrrolidone. The slurry was cast on the Al foil by Doctor Blade© technique. 10 mm round electrodes were cut out of the foil, weighed and dried at 120°C under vacuum for 4 hours to remove the residual water and solvent. Electrochemical evaluation of the materials was performed in two-electrode Swagelok cells, assembled in an Ar-filled glovebox (MBraun, Germany). Li-foil was exploited as a counter electrode (anode). The solution of 1M $LiPF_6$ in EC:DMC (1:1 vol.) served as an electrolyte. Borosilicate glass fiber was used as a separator. Galvanostatic

cycling with potential limitation (GCPL) and cyclic voltammetry (CV) measurements were carried out on Biologic VMP-3 (EC-Lab) at room temperature.

Results and discussion

Crystal structure of $LiNaCo_{0.5}Fe_{0.5}PO_4F$

The $LiNaCo_{0.5}Fe_{0.5}PO_4F$ sample for the structure refinement was obtained by a conventional solid-state route as described above. The phase analysis of the sample using SXPD data revealed minor amounts of $LiCo_{0.5}Fe_{0.5}PO_4$ (2.3 wt. %) and Li_3PO_4 (1.4 wt. %) impurities. The ratio of Co, Fe and P was determined by EDX from 40 spectra to be 0.52(3):0.48(3):1.17(6) respectively that is close to the ascribed formula. The unit cell and space symmetry were confirmed by electron diffraction (Figure 1). The derived reflection conditions are 0*kl*: $k + l = 2n$, and *hk*0: $h = 2n$ and corroborate the *Pnma* (#62) space group. The reflections which do not match these reflection conditions, such as *h*00: $h = 2n + 1$ and 00*l*: $l = 2n + 1$ in the [010] ED pattern and 0*k*0: $k = 2n + 1$ in the [001] pattern are caused by double diffraction.

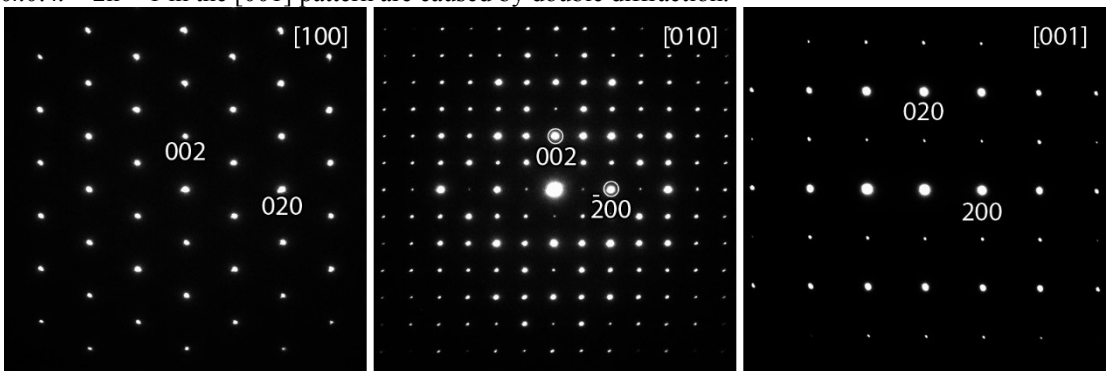

Figure 1. ED patterns of $LiNaCo_{0.5}Fe_{0.5}PO_4F$ along the [100], [010] and [001] main zone axes.

The structure of $LiNaCo_{0.5}Fe_{0.5}PO_4F$ was refined from NPD data with the use of $LiNaFePO_4F$ as a starting model [17], with $LiCo_{0.5}Fe_{0.5}PO_4$ and Li_3PO_4 admixture phases being included into the refinement. The background was fitted by a set of Legendre polynomials, followed by a refinement of the cell parameters and the peak shapes with a Pseudo-Voigt function. NPD allows locating correctly the positions of light elements, especially lithium. It is also sensitive to a Na/Li disorder and distinguishes Fe and Co sites due to different scattering lengths of these elements (9.45 and 2.49 fm respectively). After the full profile matching the scale factors, atomic coordinates and atomic displacement parameters (ADPs) were refined. Initially, ADPs were constrained to be equal for the sites occupied by a particular element and at the final stages all constraints were removed. The introduction of mixed Na/Li occupancies for the alkali metal positions resulted in an insignificant disorder, so the occupancies were fixed to 1. The crystallographic parameters, positional parameters, ADPs and main interatomic distances are listed in Tables 1–3, respectively. The experimental, calculated and difference NDP profiles after the Rietveld refinement are shown in Fig. 2.

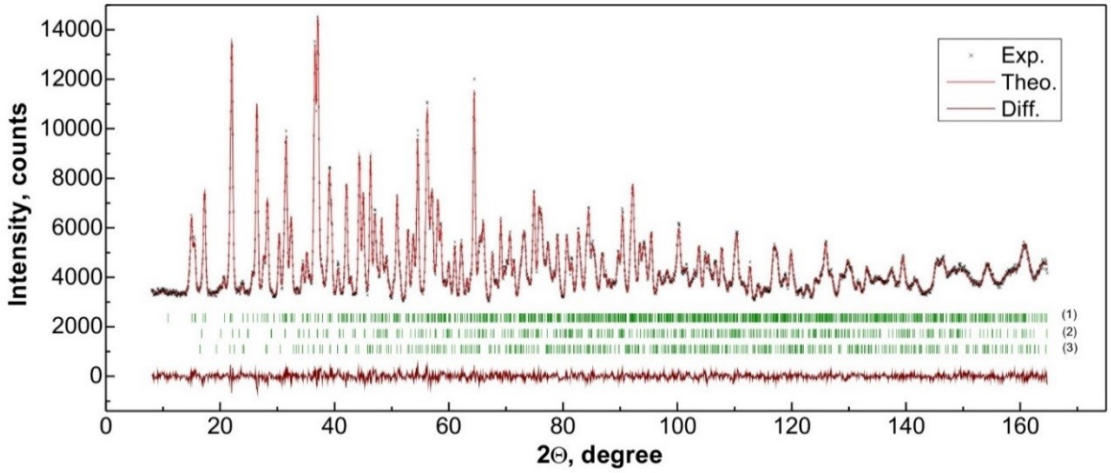

Figure 2. The experimental, calculated and difference NDP profiles after the Rietveld refinement of $LiNaCo_{0.5}Fe_{0.5}PO_4F$. The bars mark the reflection positions of the $LiNaCo_{0.5}Fe_{0.5}PO_4F$ main phase (1), $LiCo_{0.5}Fe_{0.5}PO_4$ (2) and Li_3PO_4 (3) impurities.

The crystal structure of $LiNaCo_{0.5}Fe_{0.5}PO_4F$ is shown in Fig. 3, top. Edge-shared MO_4F_2 octahedra chains, bridged by PO_4 tetrahedra, form a 3D-framework with continuous tunnels stretched along the [010] direction and cavities filled by sodium and lithium atoms, respectively. The alkali sites were found to be fully occupied by sodium and lithium. The sodium atoms (Na1) are located in continuous tunnels along the *b* axis and are coordinated with four oxygen and one fluorine atoms forming a distorted trigonal bipyramid with the average Na1–X (X = O, F) distance of 2.35 Å (Fig. 3, bottom). The Li2 environment includes four oxygen with three shorter, one longer Li-O distances, and one fluorine atom resulting in a similar bipyramidal polyhedron. If the Li3 atom is considered to be bonded with the closest three oxygens and one fluorine (within

2.1 Å), then it ends up strongly under-bonded (0.77(1) BV units). Hence, the coordination number of Li3 should be increased by the addition of O5 and F2 atoms at 2.434 and 2.791 Å respectively. In this case, the BVS value approaches 0.87(1) which is closer to 1. Therefore, it may be concluded that Li3 has [5+1] coordination (Fig.3, bottom). The positions of the fluorine atoms, refined from those of the initial model, are supported by the BVS values (Table 2).

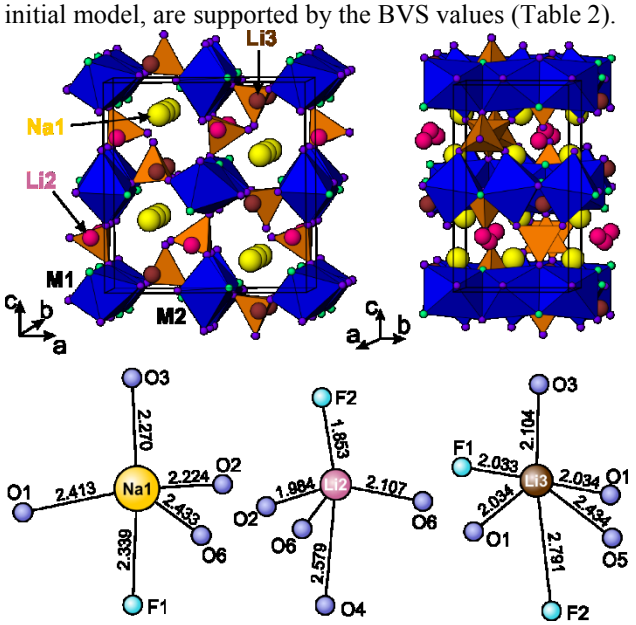

Figure 3. Top: ball-polyhedral representation of the $LiNaCo_{0.5}Fe_{0.5}PO_4F$ crystal structure. The MO_4F_2 units are depicted as blue octahedra, PO_4 units as orange tetrahedra, sodium atoms are designated as yellow (Na1), lithium – red and brown (Li2, Li3 resp.), fluorine – green, oxygen – violet spheres. Bottom: coordination environment of the alkali atoms with the bond distances (Å).

In contrast to $LiNaMPO_4F$ (M = Fe, Co) [17,29], the PO_4 tetrahedra in $LiNaCo_{0.5}Fe_{0.5}PO_4F$ are almost regular with an average P–O length equal to 1.54 Å. The MO_4F_2 octahedra are slightly distorted for both M1 and M2, though the average M–X (X = O, F) distances are the same (2.11 Å) for both MO_4F_2 octahedra. A completely random Fe/Co distribution over the M1 and M2 positions led to a twice larger ADP for the position M2 compared to that of the position M1. That is why the Fe/Co ratio was refined. The M2 site appears to be slightly more preferable for the Co atoms than the M1 site, although the Co/Fe ratio in these positions deviates from 1:1 by less than 5% only (Table 2). This small ordering partly supports the computational work [20], which demonstrated that the M2 site is likely to be occupied by Co. The partial Fe/Co ordering is corroborated by Mössbauer spectroscopy (see below) revealing two distinct Fe sites with 43/57% occupancies. It should be noted that the BVS values for the M1 and M2 cations (Table 2) are consistent with their nominal oxidation numbers supporting the refinement.

Further validation was performed by HRTEM observations. The theoretical [010] HRTEM image calculated using the parameters from Table 2 is in a fairly good agreement with the experimental one (Fig. 4).

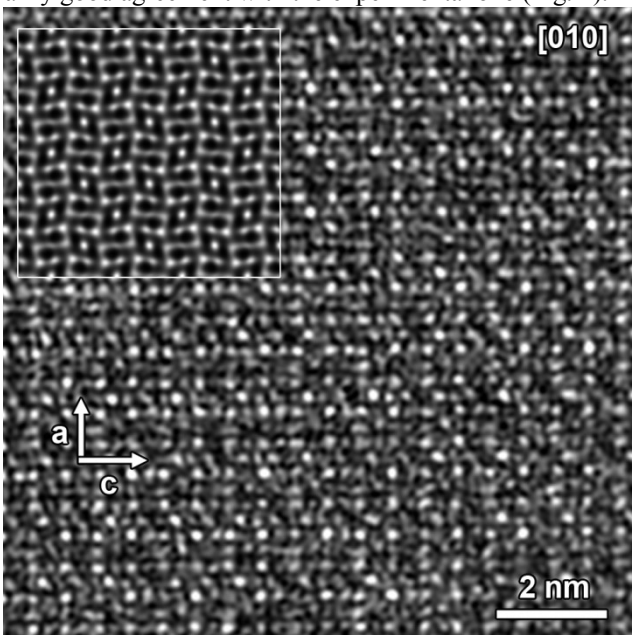

Figure 4. [010] experimental and theoretical (white square) HRTEM images.

Table 1. Crystallographic data and parameters of the structure refinement for $LiNaCo_{0.5}Fe_{0.5}PO_4F$

formula	$LiNaCo_{0.5}Fe_{0.5}PO_4F$
powder color	dark grey
space group	*Pnma* (#62)
a, Å	10.9564(2)
b, Å	6.3399(2)
c, Å	11.3926(2)
V, Å^3	791.35(3)
Z	8
density calc., g·cm^{-3}	3.49
temperature, K	293(1)
diffractometer	HRPT
radiation	neutrons, 1.494 Å
# of reflections	6383
# of ind. reflections	969
reflections used [$I \geq 2\sigma(I)$]	752
R_{int}	0.045
no. of refined parameters	100
$R_{obs}/R_p/R_{wp}$	0.0088/0.0223/0.0279
g. o. f.	1.69

Table 2. Fractional coordinates isotropic atomic displacement parameters, occupancy factors and BVS for $LiNaCo_{0.5}Fe_{0.5}PO_4F$.

Atom	*x/a*	*y/b*	*z/c*	Uiso, Å^2	Position	Occupancy	BVS
M1*	0	0	0	0.0060(7)	4*a*	0.472(3)/0.528(3)*	1.883(4)
M2*	0.5	0	0	0.0080(7)	4*b*	0.528(3)/0.472(3)*	2.056(5)
Na1	0.7754(3)	0.9913(6)	0.6535(3)	0.0134(7)	8*d*	1	1.124(5)
Li2	0.0545(1)	0.75	0.7319(11)	0.028(2)	4*c*	1	0.92(2)
Li3	0.275(1)	0.25	0.5816(12)	0.028(2)	4*c*	1	0.87(1)
P1	0.7539(3)	0.75	0.9227(3)	0.0064(6)	4*c*	1	4.91(2)
P2	0.0411(3)	0.25	0.7417(3)	0.0124(8)	4*c*	1	4.91(2)
O1	0.8191(2)	0.9498(4)	0.9649(2)	0.0111(5)	8*d*	1	2.05(1)
O2	0.7342(3)	0.75	0.7894(3)	0.0137(7)	4*c*	1	1.85(2)
O3	0.1812(3)	0.25	0.7427(3)	0.0121(7)	4*c*	1	1.93(2)
O4	0.6256(3)	0.75	0.9839(3)	0.0096(6)	4*c*	1	2.01(2)
O5	-0.0087(3)	0.25	0.8686(2)	0.0113(6)	4*c*	1	1.94(1)
O6	-0.0069(3)	0.4495(3)	0.6795(2)	0.0102(4)	8*d*	1	2.07(2)
F1	0.8710(3)	0.75	0.5282(3)	0.0131(7)	4*c*	1	0.970(6)
F2	0.0604(3)	0.75	0.8945(3)	0.0167(9)	4*c*	1	0.971(9)

* - mixed Co/Fe occupation

Table 3. Selected interatomic distances for $LiNaCo_{0.5}Fe_{0.5}PO_4F$.

Bond	Interatomic distance, Å	Bond	Interatomic distance, Å
M1–O1 (×2)*	2.046(2)	M2–O4 (×2)	2.107(2)
M1–O5 (×2)	2.182(2)	M2–O6 (×2)	2.072(2)
M1–F2 (×2)	2.096(2)	M2–F1 (×2)	2.148(2)
P1–O1 (×2)	1.532(3)	P2–O3	1.535(4)
P1–O2	1.534(4)	P2–O5	1.545(5)
P1–O4	1.569(4)	P2–O6(×2)	1.542(3)
Na1–O1	2.413(4)	Li3–O1 (×2)	2.034(5)
Na1–O2	2.224(4)	Li3–O3	2.104(13)
Na1–O3	2.270(4)	Li3–O5	2.434(12)
Na1–O6	2.433(4)	Li3–F1	2.033(12)
Na1–F1	2.339(4)	Li3–F2	2.791(13)
Li2–O2	1.984(12)	Li2–O6 (×2)	2.107(5)
Li2–O4	2.579(12)	Li2–F2	1.853(12)

Mössbauer spectroscopy

$LiNaCo_{0.5}Fe_{0.5}PO_4F$ was characterized by Mössbauer spectroscopy at room temperature. The spectrum of the sample prepared by solid-state method is presented in Figure 5. The hyperfine Mössbauer parameters [the isomeric shift (δ), the full width at half maximum (Γ), and quadruple splitting (Δ)] are given in Table 4. The spectrum was fitted with two doublets corresponding to the Fe^{2+} iron cations in the M1 and M2 octahedral sites with close, but slightly different, hyperfine parameters and spectral contributions (Table 4), which is in a good agreement with the structural refinement results. The components attributed to other iron states like Fe^{3+} were not detected in the sample spectrum. These data, coupled with the NPD refinement results, indicate no alkali metal vacancies that confirms the $LiNaCo_{0.5}Fe_{0.5}PO_4F$ formula.

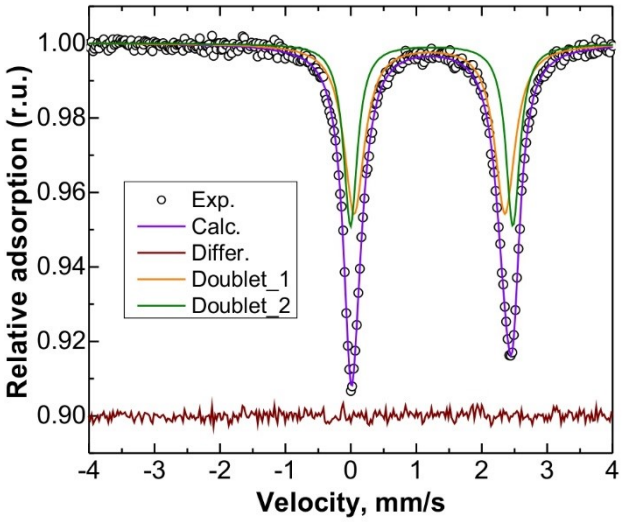

Figure 5. Mössbauer spectrum of $LiNaCo_{0.5}Fe_{0.5}PO_4F$, collected at 300K.

Table 4. ^{57}Fe Mössbauer spectrum parameters for $LiNaCo_{0.5}Fe_{0.5}PO_4F$.

Component	δ, mm/s ±0.02	Δ, mm/s ±0.02	Γ, mm/s ±0.01	Relative contribution, % ±2
Doublet_1	1.21	2.31	0.38	57
Doublet_2	1.24	2.49	0.26	43

Electrochemical tests

The solid-state prepared material exhibited extremely poor electrochemical activity, therefore for the electrochemical evaluation, $LiNaCo_{0.5}Fe_{0.5}PO_4F$ cathode materials were synthesized via the freeze-drying route. Li_3PO_4 and metallic Co were detected as minor impurities (4 and 6 wt. % respectively). The carbon content was estimated by thermogravimetric analysis to be 9.4 wt. %, which were factored into calculations of the gravimetric capacity along with the impurities. It is interesting to analyze and compare the morphology and particle sizes of materials prepared by two different techniques. The solid-state synthesis resulted in huge "fused" agglomerates of particles larger than 10÷20 μm (Fig. 6a). The freeze-drying method led to a drastic change in the morphology with a significant shrinkage of the particle sizes. In this case, the material consisted of 50÷150 nm particles (Fig. 6b, c). This effect can be explained by a high degree of homogenization as well as the influence of the residual carbon, which hinders both growth and agglomeration of the particles.

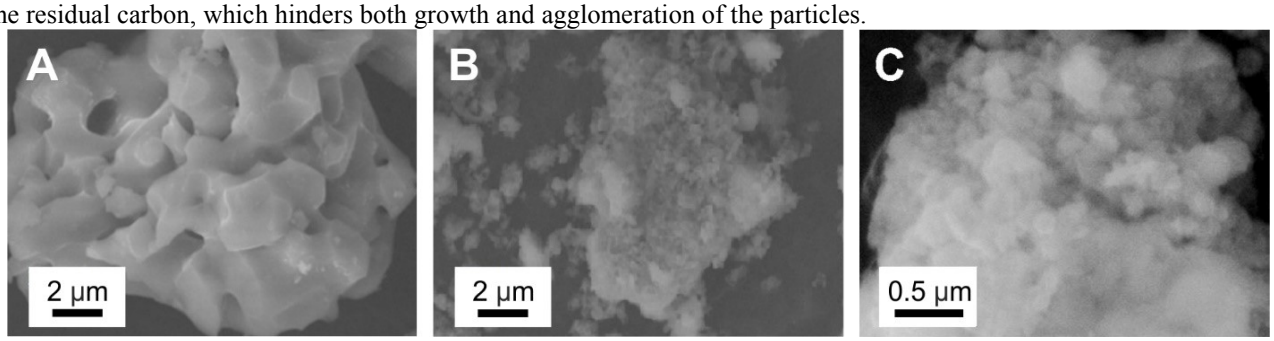

Figure 6. SEM images of $LiNaCo_{0.5}Fe_{0.5}PO_4F$ synthesized by conventional solid-state (a) and freeze-drying assisted methods with 10K amplification (b) and 50K amplification (c).

The electrodes were tested by GCPL and CV techniques in a two-electrode cell with metallic Li as a counter electrode. $LiNaCo_{0.5}Fe_{0.5}PO_4F$ demonstrated a reversible Li-ion intercalation under galvanostatic cycling in the 2.4÷5.1 V vs Li/Li^+ range. The first charge process occurs at higher potentials than the subsequent ones, while the first and following discharge curves are almost the same (Figure 7, left). A higher voltage upon first charging evidences that it is more difficult for the

larger Na^+ to be removed from the structure. After the extraction of Na^+ ions, Li ions are mainly de/intercalated during subsequent charge/discharge processes agreeing with the change of the curve shape and indicated by cyclic voltammetry as well (Figure 7, right). In fact, the distinctive behavior in the first cycle is characteristic of many Na-containing fluoride-phosphates cycled in a Li cell, like 3D-$NaLiFePO_4F$ or layered Na_2FePO_4F and attributed to the extraction of Na with a consecutive de/intercalation of Li ions [14,17], which was confirmed by XRD and EDX measurements on cycled electrodes demonstrated the complete Na removal.

The redox activity attributed to the Fe^{3+}/Fe^{2+} transition is almost fully reversible with the average potential located at ~3.4 V vs Li/Li^+, still the Co^{3+}/Co^{2+} transition is characterized by a less reversibility and minor cathodic response compared to the corresponding anodic activity which might be ascribed mostly to the electrolyte decomposition at high voltages. Moreover, at potentials over 5 V, the $LiNaCo_{0.5}Fe_{0.5}PO_4F$ cathode material exhibits a serious capacity fading (Figure 7, left). A raise of the cut-off potentials up to 5.2 and 5.3 V vs Li/Li^+ (Figure 7, right) weakly affects the Fe^{3+}/Fe^{2+} cathodic activity but results in a growing Co^{3+}/Co^{2+} discharge capacity. Under these conditions, the average Co^{3+}/Co^{2+} potential cannot be clearly defined. It might be seen that Co^{2+} starts oxidizing at slightly higher potentials than in Li_2CoPO_4F [18,19].

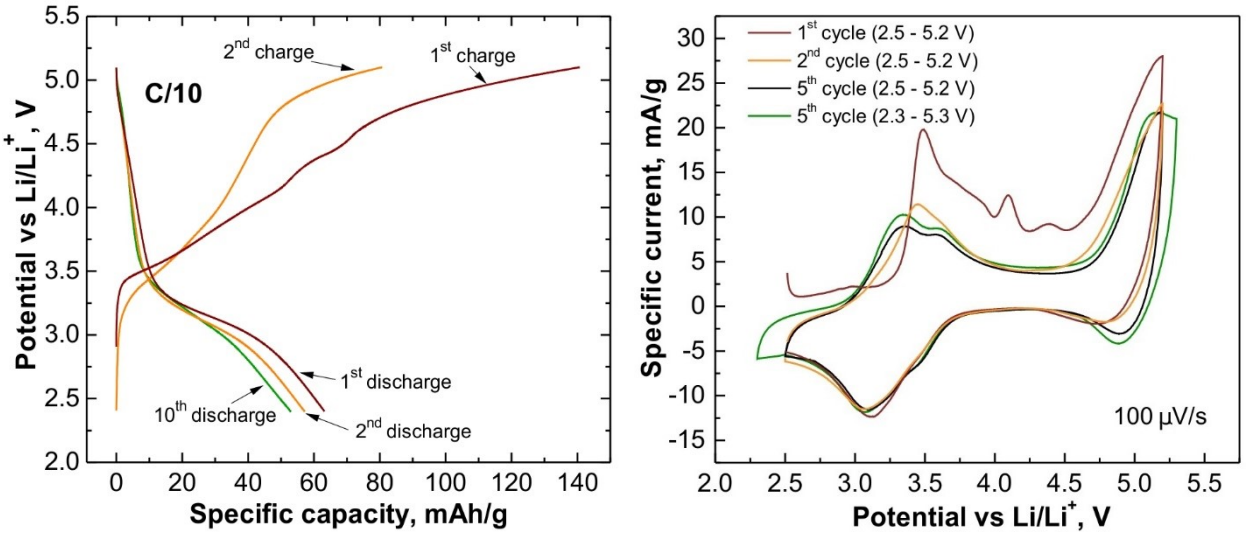

Figure 7. Left. Charge/discharge curves of $LiNaCo_{0.5}Fe_{0.5}PO_4F$ within 2.4÷5.1 V vs Li/Li^+ range at C/10. Right. $LiNaCo_{0.5}Fe_{0.5}PO_4F$ cyclic voltammograms within different potential ranges at a scan rate of 100 µV/s.

This increase of the Co^{3+}/Co^{2+} charge potentials in the mixed $LiNaCo_{0.5}Fe_{0.5}PO_4F$ can be explained in terms of changes in the bond distances. Assuming that Co and Fe are randomly distributed in the structure, some $Co^{2+}O_4F_2$ octahedra are neighbored by one or two $Fe^{2+}O_4F_2$ octahedra with 75% or 25% probability respectively. Initially, M–X bond distances are equal for both metals. On charge, Fe^{2+} ions oxidize first turning into Fe^{3+} with a smaller ionic radius (0.78 Å vs 0.645 Å respectively [30]), leading to a shrinkage of the Fe^{3+}–X distances with an extension of the Co^{2+} octahedron (Figure 8). As a result, Co^{2+}–X distances stretch and induce a shift of the Co^{3+}/Co^{2+} potential to higher values. However, it should be noticed that the potentials corresponding to the Co^{3+}/Co^{2+} redox activity for $Li_{2-x}Co_{0.5}Fe_{0.5}PO_4F$ and $Li_{2-x}CoPO_4F$ with the same Li content (*x* value) are higher for the latter phase due to a greater electronegativity of Co vs Fe. A similar influence of the M–X bond length on the redox potential was clearly demonstrated experimentally and computationally for $LiFeSO_4F$ triplite and tavorite polymorphs [7, 31], evidencing that the 0.3 V raise for the triplite partly originates from a slight elongation of the average Fe^{2+}–O bond distance [32].

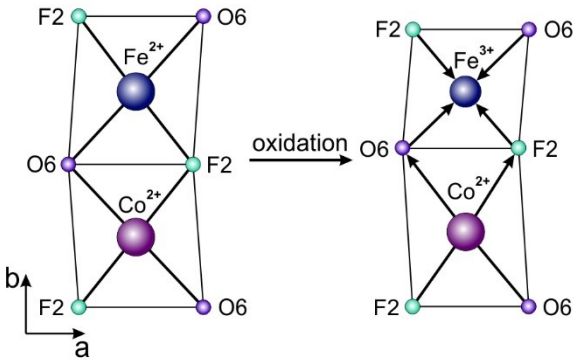

Figure 8. Graphical representation of the changes in M–X (X = O, F) bond distances during the deintercalation process. Arrows designate the directions of bond distance changes.

The next step was to examine the $LiNaCo_{0.5}Fe_{0.5}PO_4F$ cathode material in the 2.4÷4.6 V vs Li/Li^+ range, which covers mostly the Fe^{3+}/Fe^{2+} redox activity. At C/20 the material is capable to deliver more than 55 mAh/g corresponding to 82% of the theoretical capacity regarding to Fe^{3+}/Fe^{2+} (67 mAh/g) with a good capacity retention and sloping voltage profile suggesting a one-phase de/intercalation mechanism favorable for rapid kinetics (Figure 9, left). The material also retains a significant amount of the initial capacity with increasing C-rates (Figure 9, right).

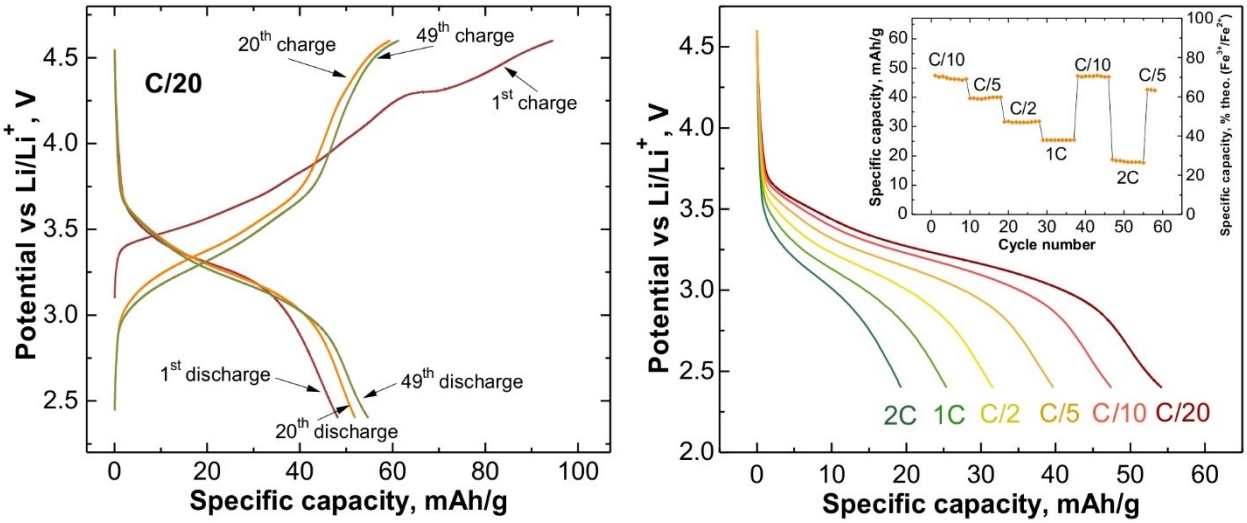

Figure 9. Left. Charge/discharge curves of $LiNaCo_{0.5}Fe_{0.5}PO_4F$ within the 2.4÷4.6 V vs Li/Li^+ range at C/20. Right. Charge/discharge curves of $LiNaCo_{0.5}Fe_{0.5}PO_4F$ at various C-rates. The inset demonstrates the capacity vs cycle number dependence at different C-rates.

Conclusions

We succeeded to synthesize the mixed $LiNaCo_{0.5}Fe_{0.5}PO_4F$ fluoride-phosphate by conventional solid-state and freeze-drying methods. The crystal structure was refined based on the neutron powder diffraction data revealing a complete alkali metal ordering within three crystallographic sites, and a small degree of ordering of Fe and Co at the transition metal sites. One-step freeze-drying synthesis resulted in a material with nano-sized morphology in comparison to that of two-step solid-state synthesis. This material efficiently deintercalates Na^+ and intercalates Li^+ involving an Fe^{3+}/Fe^{2+} redox activity centered at 3.4 V (vs Li/Li^+). Capable of delivering a reversible capacity approaching 82 % of the theoretical value (regarding to Fe^{3+}/Fe^{2+}), the material exhibits stable cycling within the 2.4÷4.6 V vs Li/Li^+ range at increasing C-rates up to 2C. The redox activity corresponding to the Co^{3+}/Co^{2+} transition in the material takes place over 4.9 V (vs Li/Li^+) which is slightly higher than in the pure Li_2CoPO_4F. Unfortunately, a thorough investigation of the subtle effects of Fe for Co substitution on the operating potentials in the orthorhombic $LiNaCo_{0.5}Fe_{0.5}PO_4F$ fluoride-phosphate is now hindered by degradation processes occurring at high voltages in most commercially available electrolytes.

Acknowledgements

The authors kindly thank Dr. O. A. Shlyakhtin for the assistance in the freeze-drying synthesis. We are grateful to the Laboratory for Neutron Scattering and Imaging (NLS) at the Paul Scherrer Institut (Villigen, Switzerland) for granting beam time at the HRPT diffractometer and to Dr. D. V. Sheptyakov for the technical support during the experiment. The work was partly supported by Russian Foundation for Basic Research (RFBR grant 13-03-00495a, 14-29-04064 ofi_m, 16-33-01131 mol_a), Skoltech Center for Electrochemical Energy Storage and Moscow State University Development Program up to 2020. J. Hadermann, O.M. Karakulina and A.M. Abakumov acknowledge support from FWO under grant G040116N.

References

1. M. S. Whittingham, Lithium batteries and cathode materials, Chem. Rev. 104 (2004) 4271–4301.
2. J. B. Goodenough and Y. Kim, Challenges for Rechargeable Li Batteries, Chem. Mater. 22 (2010) 587–603.
3. A. R. Cho, J. N. Son, V. Aravindan, H. Kim, K. S. Kang, W. S. Yoon, W. S. Kim, Y. S. Lee, Carbon supported, Al doped-$Li_3V_2(PO_4)_3$ as a high rate cathode material for lithium-ion batteries, J. Mater. Chem. 22 (2012) 6556-6560.
4. A. Yamada, N. Iwane, S.-i. Nishimura, Y. Koyama, I. Tanaka, Synthesis and electrochemistry of monoclinic $Li(Mn_xFe_{1-x})BO_3$: a combined experimental and computational study, J. Mater. Chem. 21 (2011) 10690–10696.
5. M. R. Roberts, G. Vitins, G. Denuault, J. R. Owen, High Throughput Electrochemical Observation of Structural Phase Changes in $LiFe_{1-x}Mn_xPO_4$ during Charge and Discharge, J. Electrochem. Soc. 157 (2010) A381-A386.
6. N. V. Kosova, O. A. Podgornova, E. T. Devyatkina, V. R. Podugolnikov and S. A. Petrov, Effect of Fe^{2+} substitution on the structure and electrochemistry of $LiCoPO_4$ prepared by mechanochemically assisted carbothermal reduction, J. Mater. Chem. A 2 (2014) 20697–20705.

7. P. Barpanda, M. Ati, B. C. Melot, G. Rousse, J.-N. Chotard, M.-L. Doublet, M. T. Sougrati, S. A. Corr, J.-C. Jumas, J. M. Tarascon, A 3.90 V Iron-Based Fluorosulphate Material for Lithium-Ion Batteries Crystallizing in the Triplite Structure, Nat. Mater. 10, (2011) 772−779.
8. M. Ati, B. C. Melot, G. Rousse, J.-N. Chotard, P. Barpanda, J. M. Tarascon, Structural and Electrochemical Diversity in $LiFe_{1-\delta}Zn_{\delta}SO_4F$ Solid Solution: A Fe-Based 3.9 V Positive-Electrode Material, Angew. Chem. Int. Ed. 50 (2011) 10574–10577.
9. C. Masquelier, L. Croguennec, Polyanionic (Phosphates, Silicates, Sulfates) Frameworks as Electrode Materials for Rechargeable Li (or Na) Batteries, Chem. Rev. 113 (2013) 6552–6591.
10. G. Rousse, J. M. Tarascon, Sulfate-Based Polyanionic Compounds for Li-Ion Batteries: Synthesis, Crystal Chemistry, and Electrochemistry Aspects Chem. Mater. 26 (2014) 394–406.
11. J. Barker, M. Y. Saidi, J. L. Swoyer, Electrochemical Insertion Properties of the Novel Lithium Vanadium Fluorophosphate, $LiVPO_4F$, J. Electrochem. Soc. 150 (2003) A1394−A1398.
12. J. Barker, M. Y. Saidi, and J. L. Swoyer, A Sodium-Ion Cell Based on the Fluorophosphate Compound $NaVPO_4F$, Electrochemical and Solid-State Letters 6 (2003) A1-A4.
13. N. Recham, J-N. Chotard, J-C. Jumas, L. Laffont, M. Armand, J-M. Tarascon, Ionothermal Synthesis of Li-Based Fluorophosphates Electrodes Chem. Mater. 22 (2010)1142–1148.
14. B. L. Ellis, W. R. M. Makahnouk, W. N. R. Weetaluktuk, D. H. Ryan, L. F. Nazar, Crystal Structure and Electrochemical Properties of A_2MPO_4F Fluorophosphates (A = Na, Li; M = Fe, Mn, Co, Ni), Chem. Mater. 22 (2010) 1059–1070.
15. S. Okada, M. Ueno, Y. Uebou, J. Yamaki, Fluoride Phosphate Li_2CoPO_4F as a High-Voltage Cathode in Li-Ion Batteries. J. Power Sources 146 (2005) 565−569.
16. S.-W. Kim, D.-H. Seo, H. Kim, K.-Y. Park, K. A Kang, Comparative Study on Na_2MnPO_4F and Li_2MnPO_4F for Rechargeable Battery Cathodes. Phys. Chem. Chem. Phys. 14 (2012) 3299–3303.
17. N. R. Khasanova, O. A. Drozhzhin, D. A. Storozhilova, C. Delmas, E. V. Antipov, New form of Li_2FePO_4F as cathode material for Li-ion batteries Chem. Mater., 24 (2012) 4271–4273.
18. N. R. Khasanova, A. N. Gavrilov, E. V. Antipov, K. G. Bramnik, H. Hibst, Structural Transformation of Li_2CoPO_4F upon Li-Deintercalation. J. Power Sources 196 (2011) 355–360.
19. S. Amaresh, G. J. Kim, K. Karthikeyan, V. Aravindan, K. Y. Chung, B. W. Choc, Y. S. Lee, Synthesis and enhanced electrochemical performance of Li_2CoPO_4F cathodes under high current cycling, Phys.Chem.Chem.Phys., 14 (2012) 11904–11909.
20. F. Yang, W. Sun, Y. Li, H. Yuan, Z. Dong, H. Li, J. Tian, Y. Zheng, J. Zhang, Li_2FePO_4F and its metal-doping for Li-ion batteries: an ab initio study RSC Adv. 4 (2014) 50195–50201.
21. N. R. Khasanova, O. A. Drozhzhin, S. S. Fedotov, D. A. Storozhilova, R. V. Panin, E. V. Antipov, Synthesis and electrochemical performance of $Li_2Co_{1-x}M_xPO_4F$ (M = Fe, Mn) cathode materials, Beilstein J. Nanotechnol. 4 (2013) 860–867.
22. E. V. Antipov, N. R. Khasanova, S. S. Fedotov, Perspectives on Li and transition metal fluoride phosphates as cathode materials for a new generation of Li-ion batteries, IUCrJ 2 (2015) 85-94.
23. O. A. Shlyakhtin, Y. S. Yoon, S. H. Choi, Y.-J. Oh, Freeze drying synthesis of $LiNi_{0.5}Mn_{0.5}O_2$ cathode materials, Electrochim. Acta 50 (2004) 505–509.
24. S. J. Shi, J. P. Tu, Y. Y. Tang, Y. X. Yu, Y. Q. Zhang, X. L. Wang, Synthesis and electrochemical performance of $Li_{1.131}Mn_{0.504}Ni_{0.243}Co_{0.122}O_2$ cathode materials for lithium ion batteries via freeze drying, J. Power Sources 221 (2013) 300–307.
25. C. Wang, H. Liu, W. Yang, An integrated core–shell structured $Li_3V_2(PO_4)_3$@C cathode material of LIBs prepared by a momentary freeze-drying method, J. Mater. Chem. 22 (2012) 5281–5285.
26. D. Wang, Z. Wang, X. Huang, L. Chen, Continuous solid solutions $LiFe_{1-x}Co_xPO_4$ and its electrochemical performance, J. Power Sources 146 (2005) 580–583.
27. V. Petricek, M.Dusek, L. Palatinus, Crystallographic Computing System JANA2006: General Features. Z. Kristallogr. 229 (2014) 345–352.
28. S. A. Bruggemann, Y. A. Artzybashev, S. V. Orlov, 1993, UNIVEM, Version 4.5.
29. H. Ben Yahia, M. Shikano, S. Koike, K. Tatsumi, H. Kobayashi, H. Kawaji, M. Avdeev, W. Miiller, C. D. Ling, J. Liu, M.-H. Whangbo, Synthesis and Characterization of the Crystal Structure and Magnetic Properties of the New Fluorophosphate $LiNaCo[PO_4]F$, Inorg. Chem. 51 (2012) 8729–8738.
30. R. D. Shannon, Revised Effective Ionic Radii and Systematic Studies of Interatomic Distances in Halides and Chalcogenides, Acta Cryst. A 32 (1976) 751–767.
31. N. Recham, J.-N. Chotard, L. Dupont, C. Delacourt, W. Walker, M. Armand, J.-M. Tarascon, A 3.6 V Lithium-Based Fluorosulphate Insertion Positive Electrode for Lithium-Ion Batteries, Nat. Mater. 9 (2010) 68–74.
32. S. C. Chung, P. Barpanda, S.-i. Nishimura, Y. Yamada, A. Yamada, Polymorphs of $LiFeSO_4F$ as cathode materials for lithium ion batteries – a first principle computational study, Phys. Chem. Chem. Phys. 14 (2012) 8678–8682.